**THE EFFECT OF INERTIA FORCES ON SHEAR DRIVEN FLOW BETWEEN THE HULL SURFACE OF A VESSEL AND ICE FLOES IN THE ICE SLIDING PHASE**

Jorma Kämäräinen

Journal of Structural Mechanics
Vol. 40, No. 4, 2007, pp. 40 - 54

## SUMMARY

The purpose of this study is to investigate theoretically the pressure field resulting from the flow in the gap between the hull of a ship and fully submerged ice floes over which the hull slides when the ship is moving at a constant speed in a level ice field. A computer code Iceflo has been written to calculate the flow in a converging-diverging gap between the hull surface of a moving vessel and an ice floe. The calculations indicate that the inertia effects have an important role when calculating the pressure distribution in the gap between the hull surface of a ship and ice floes.

## INTRODUCTION

It is assumed that a ship moves in a level ice field at a constant speed $v$. Four different phases in the icebreaking process can be discerned in the time domain, following the time history of the movement of the ice floes (Valanto (1989) and Puntigliano (1995) and (2000)): the breaking phase; the rotative phase; the sliding phase, and the final phase. The first three phases, which take place at the bow area of a ship, are depicted in Figure 1.

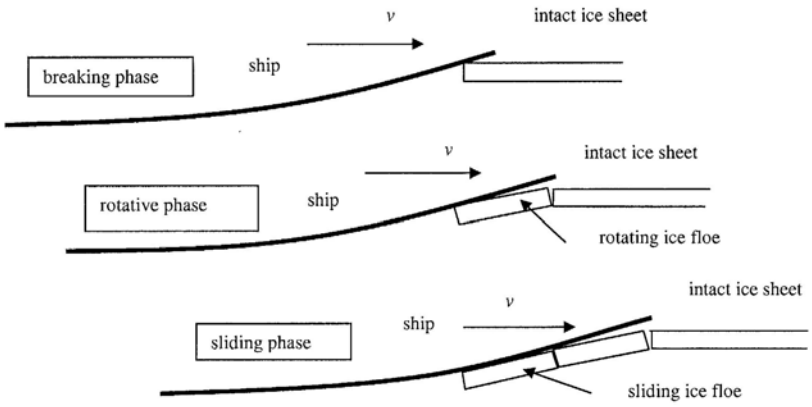


**Figure 1.** The first three phases of the icebreaking process (according to Puntigliano (2000), Figure 3).

The purpose of this study is to investigate theoretically the pressure field resulting from the flow in the gap between the hull of a ship and fully submerged ice floes over which the hull slides when the ship is moving at a constant speed in a level ice field.

## THE CALCULATION PROBLEM

The aim is to develop a numerical calculation method to determine the steady or unsteady shear-driven flow velocity and pressure fields in a converging-diverging gap between the hull surface and a rectangular ice floe, as shown in Figure 2. The upper drawing in Figure 2 depicts the gap between a rectangular ice floe and a convex hull form. The origin is placed in the middle of the contact area of the hull surface and the ice floe. The gap has a height, $h$, which is a function of $x$ and $y$. The length and breadth of the ice floe are $l$ and $b$. The hull surface has a radius of curvature, $R_x$, in the $x$-coordinate direction and $R_y$ in the $y$-coordinate direction. The hull surface moves at a speed, $U$, in the positive $x$-axis direction and the speed of the ice floe is assumed to be zero. The hull surface is thus the driving surface for the shear-driven flow in the gap between the two surfaces. The hull surface and the surface of the ice floe are assumed to be perfectly smooth. The fluid in the gap is assumed to be water at a constant temperature with constant density and viscosity.

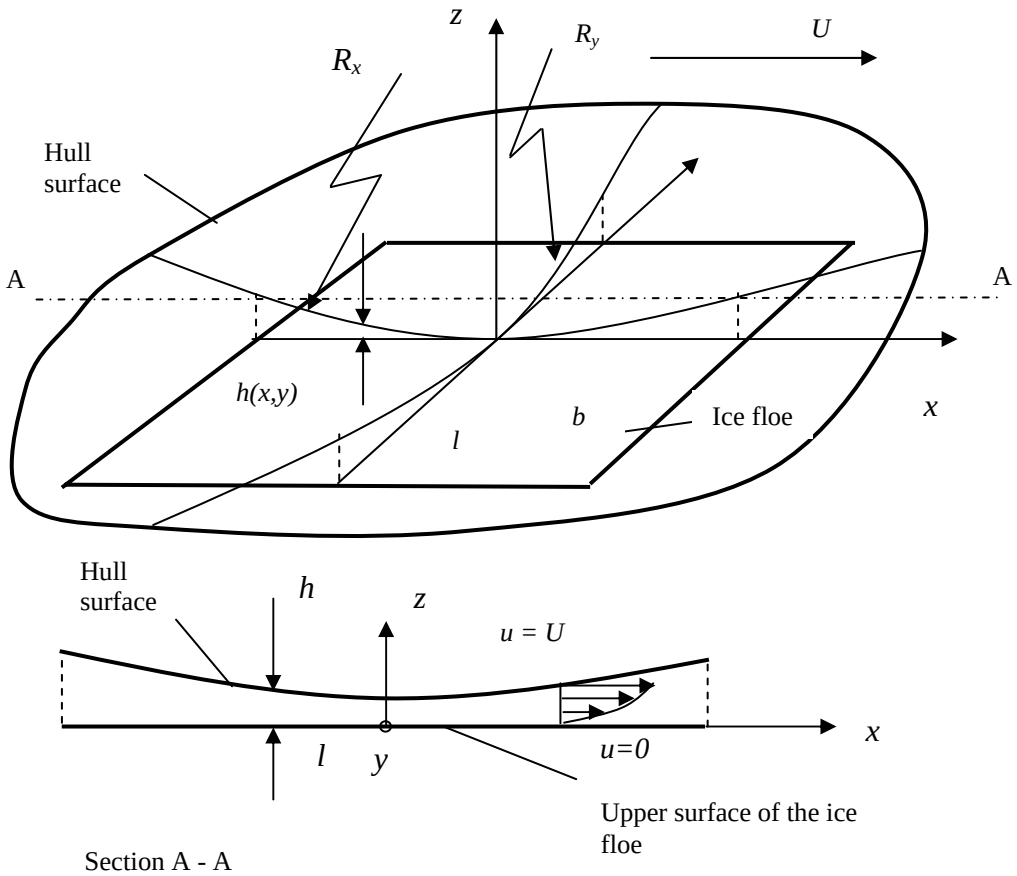


**Figure 2.** The geometry considered in the study.

The lower drawing in Figure 2 depicts a section, A-A, of the gap between the ice floe and the hull surface. A flow is generated in the gap as a result of the motion of the hull surface. On the surface of the ice floe the flow has a velocity of zero and on the hull surface the flow velocity equals the speed of the hull surface as a result of the no-slip boundary conditions on the solid surfaces. The flow field and the pressure in the gap depend on the boundary conditions at the edges of the ice floe.

The problem is further simplified by assuming that the tangential velocity of the hull surface equals $U$, since the radius of the hull surface, $R_x$, is much larger than the length of the ice floe, $l$.

The nature of the flow in the gap can be characterized by two dimensionless numbers, the Couette Reynolds number and the reduced Reynolds number. The Couette Reynolds number, $\mathrm{Re}_C$, is defined as:

$$\mathrm{Re}_C = \frac{Uh}{2\nu} \tag{1}$$

where $\nu$ is the kinematic viscosity of the fluid, $\nu = \eta / \rho$, where $\eta$ is the molecular viscosity, and $\rho$ is the density of the fluid. According to experiments, a Couette flow, i.e. flow between two parallel plates in relative motion is turbulent, if $\mathrm{Re}_C$ >1300 (see e.g. Schlichting and Gersten (2000)).

The reduced Reynolds number, Re*, is defined as the ratio of viscous forces to inertia forces:

$$\mathrm{Re}^* = \frac{Ul}{\nu}\left(\frac{h}{l}\right)^2 = \mathrm{Re}_C\left(\frac{2h}{l}\right), \tag{2}$$

where $l$ is the length of the ice floe. The inertia forces can be neglected with respect to the viscous forces, if the reduced Reynolds number $\mathrm{Re}^* \ll 1$.

The analysis for the flow in the gap for a typical hull form, based on calculation of the Couette Reynolds number and the reduced Reynolds number, indicated that the calculation method has to be able to model time dependent laminar and turbulent flow with inertia effects, see Kämäräinen (2007).

## THE EQUATIONS

The Reynolds averaged Navier-Stokes (RANS) equations with constant density and viscosity are:

$$\rho \frac{\partial \overline{u}_i}{\partial t} + \rho \frac{\partial}{\partial x_j}\left(\overline{u}_j \overline{u}_i\right) = -\frac{\partial \overline{p}_d}{\partial x_i} + \eta \frac{\partial^2 \overline{u}_i}{\partial x_j \partial x_j} - \rho \frac{\partial}{\partial x_j}\left(\overline{u_j' u_i'}\right) \tag{3}$$

$$\frac{\partial \overline{u}_i}{\partial x_i} = 0\,, \tag{4}$$

where $\overline{u}_i$ are the mean velocity components, $\overline{p}_d$ is the mean dynamic pressure, $\rho\overline{u_j' u_i'}$ are the Reynolds stresses, and $t$ is time. Equations (3) and (4) can be simplified by making the boundary layer approximations, assuming that $h \ll l$ and $h \ll b$, and that the pressure in the boundary layer is constant in the vertical direction along the $z$-axis. Taking these assumptions into account, the RANS Equations (3) and (4) can be written in Cartesian coordinates as follows, known also as Prandtl's turbulent boundary-layer equations:

$$\rho \frac{\partial \overline{u}}{\partial t} + \frac{\partial}{\partial x}\left(\overline{u}\,\overline{u}\right) + \rho \frac{\partial}{\partial y}\left(\overline{v}\,\overline{u}\right) + \rho \frac{\partial}{\partial z}\left(\overline{w}\,\overline{u}\right) = -\frac{\partial \overline{p}_d}{\partial x} + \eta \frac{\partial^2 \overline{u}}{\partial z^2} - \rho \frac{\partial}{\partial z}\left(\overline{w'u'}\right) \tag{5}$$

$$\rho \frac{\partial \overline{v}}{\partial t} + \frac{\partial}{\partial x}\left(\overline{u}\,\overline{v}\right) + \rho \frac{\partial}{\partial y}\left(\overline{v}\,\overline{v}\right) + \rho \frac{\partial}{\partial z}\left(\overline{w}\,\overline{v}\right) = -\frac{\partial \overline{p}_d}{\partial y} + \eta \frac{\partial^2 \overline{v}}{\partial z^2} - \rho \frac{\partial}{\partial z}\left(\overline{w'v'}\right) \tag{6}$$

$$0 \approx -\frac{\partial \overline{p}_d}{\partial z} \tag{7}$$

$$\frac{\partial \overline{u}}{\partial x} + \frac{\partial \overline{v}}{\partial y} + \frac{\partial \overline{w}}{\partial z} = 0\,, \tag{8}$$

where $\overline{u}, \overline{v}$ and $\overline{w}$ is the mean velocity of the flow in the directions of the $x$-, $y$- and $z$-coordinate axes. Equation (7) indicates that the pressure is constant across the fluid film, i.e.

$$\overline{p}_d = \overline{p}_d\left(x, y, t\right). \tag{9}$$

Equations can be further simplified by integrating them across the gap height, $h$, see Kämäräinen (2007). In this way the dimensions of the calculation problem can be reduced from three to two, which greatly simplifies the numerical calculation procedure. We now get the equations of Constantinescu, which describe laminar two-dimensional flow with inertia effects in a gap between the hull surface and an ice floe:

$$\rho \frac{\partial\left(u_m h\right)}{\partial t} + \rho \frac{\partial}{\partial x}\left(\alpha u_m^2 h + \beta U^2 h - \gamma u_m U h\right) + \rho \frac{\partial}{\partial y}\left(\alpha u_m v_m h - \delta U v_m h\right) + \\ + h \frac{\partial \overline{p}_d}{\partial x} + \frac{\eta k_x}{h}\left(u_m - \frac{U}{2}\right) = 0 \tag{10}$$

$$\rho\frac{\partial(v_m h)}{\partial t}+\rho\frac{\partial}{\partial x}(\alpha u_m v_m h-\delta U u_m h)+\rho\frac{\partial}{\partial y}(\alpha v_m^2 h)+h\frac{\partial \overline{p}_d}{\partial y}+\frac{\eta k_y}{h}v_m=0 \tag{11}$$

$$\frac{\partial(u_m h)}{\partial x}+\frac{\partial(v_m h)}{\partial y}+\frac{\partial h}{\partial t}=0 \tag{12}$$

where

$$\alpha=1.2,\ \beta=0.133,\ \gamma=0.2 \text{ and } \delta=0.1 \text{ and } k_x=k_y=12, \tag{13}$$

for laminar flow. These equations were originally given by Constantinescu and Galetuse (1974) for steady flow. Leschziner (1976) also presented the derivation of the equations for steady laminar flow. According to Constantinescu and Galetuse (1982), the equations can be used for calculation of turbulent flow by setting:

$$\alpha=1,\ \beta\cong 0.885\left[2\cdot \mathrm{Re}_C(x,y)\right]^{-0.367},\ \gamma=0 \text{ and } \delta\cong 1.95\left[2\cdot \mathrm{Re}_C(x,y)\right]^{-0.43}. \tag{14}$$

The turbulence model of Hirs (1973) based on bulk flow theory was used:

$$\begin{aligned} k_x &= 0.0687\left(2\cdot \mathrm{Re}_C\right)^{0.75} \\ k_y &= 0.0392\left(2\cdot \mathrm{Re}_C\right)^{0.75}. \end{aligned} \tag{15}$$

Analytical solution of equations (10), (11) and (12) is not possible, except in special cases, but a numerical solution method has to be used.

## NUMERICAL SOLUTION OF THE EQUATIONS

A computer code Iceflo was written to solve Equations (10), (11) and (12). The numerical solution method is based on the finite difference method given in Griebel *et al.* (1998). The program can be used to calculate the velocity of the flow and the pressure in the gap between the hull surface and a rectangular ice floe.

### Solution of the momentum equations

First the time dependent terms of Equations (10) and (11) are considered:

$$\rho\frac{\partial(u_m h)}{\partial t}=\rho h\frac{\partial u_m}{\partial t}+\rho u_m\frac{\partial h}{\partial t} \tag{16}$$

$$\rho\frac{\partial(v_m h)}{\partial t}=\rho h\frac{\partial v_m}{\partial t}+\rho u_m\frac{\partial h}{\partial t} \tag{17}$$

The time derivatives of $u_m$ and $v_m$ on the right hand side of Equations (16) and (17) can be discretized by using Euler's method:

$$\left[\frac{\partial u_m}{\partial t}\right]^{(n+1)} \approx \frac{u_m^{(n+1)} - u_m^{(n)}}{\Delta t} \tag{18}$$

$$\left[\frac{\partial v_m}{\partial t}\right]^{(n+1)} \approx \frac{v_m^{(n+1)} - v_m^{(n)}}{\Delta t} \tag{19}$$

where the subscript $n$ denotes the value of the variable at time $t_n$ and ($n$+1) denotes the value of the variable at the next time step $t_{n+1}$, after the period of time $\Delta t$ has passed. Using Equations (18) and (19), Equations (10) and (11) can now be written in the following form:

$$u_m^{(n+1)} = F - \frac{\Delta t}{\rho}\frac{\partial \overline{p}_d}{\partial x} \tag{20}$$

$$v_m^{(n+1)} = G - \frac{\Delta t}{\rho}\frac{\partial \overline{p}_d}{\partial y} \tag{21}$$

where

$$F := u_m^{(n)} - \frac{\Delta t}{\rho h}\left[\rho\frac{\partial}{\partial x}\left(\alpha u_m^2 h + \beta U^2 h - \gamma u_m U h\right) + \rho\frac{\partial}{\partial y}\left(\alpha u_m v_m h - \delta U v_m h\right) + \right.$$
$$\left. + \frac{\eta k_x}{h}\left(u_m - \frac{U}{2}\right) + \rho u_m \frac{\partial h}{\partial t}\right] \tag{22}$$

and

$$G := v_m^{(n)} - \frac{\Delta t}{\rho h}\left[\rho\frac{\partial}{\partial x}\left(\alpha u_m v_m h - \delta U v_m h\right) + \rho\frac{\partial}{\partial y}\left(\alpha v_m^2 h\right) + \frac{\eta k_y}{h} v_m + \rho v_m \frac{\partial h}{\partial t}\right]. \tag{23}$$

The spatial derivatives in $F$ and $G$ were calculated by replacing the first derivatives by centered differences and the second derivatives by the donor-cell discretization. If $F$ and $G$ are calculated at time $t_n$ , and $\partial \overline{p}_d / \partial x$ and $\partial \overline{p}_d / \partial y$ at time $t_{n+1}$, the following time-discretised equations of momentum are obtained:

$$u_m^{(n+1)} = F^{(n)} - \frac{\Delta t}{\rho}\frac{\partial \overline{p}_d^{(n+1)}}{\partial x} \tag{24}$$

$$v_m^{(n+1)} = G^{(n)} - \frac{\Delta t}{\rho}\frac{\partial \overline{p}_d^{(n+1)}}{\partial y}. \qquad (25)$$

A staggered rectangular grid is used to discretize equations (24) and (25) with respect to position (see Figure 3).

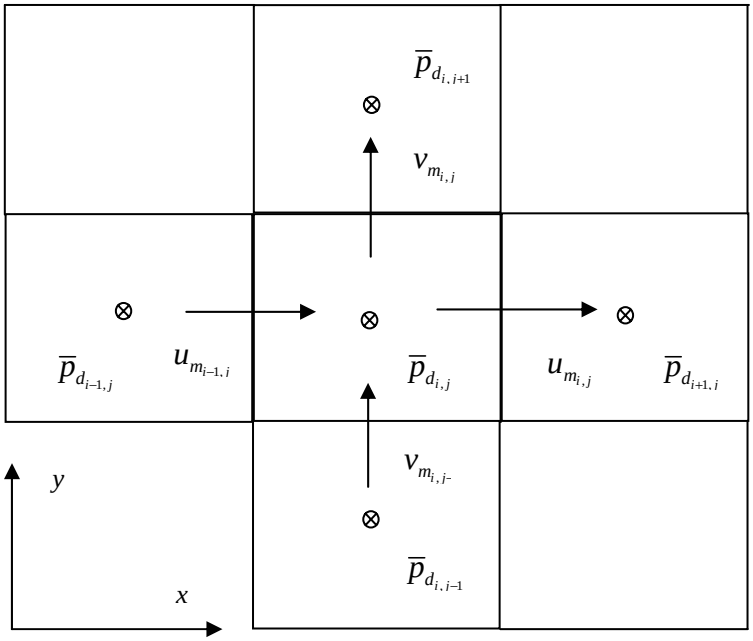


*Figure 3. Staggered grid.*

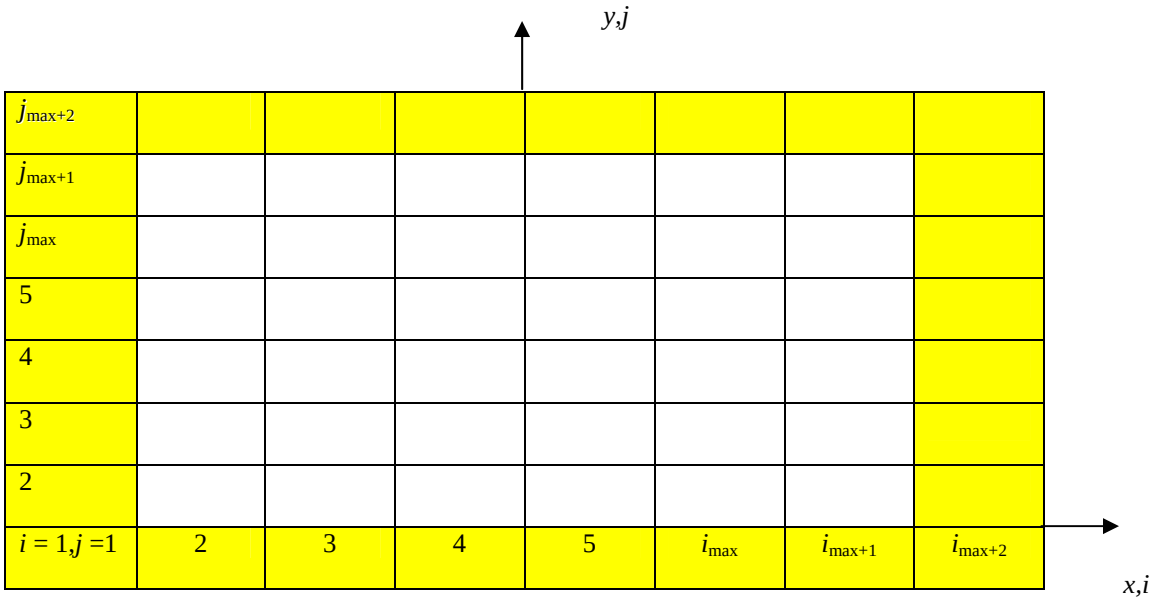


*Figure 4. Calculation domain surrounded by ghost cells ($i_{max}$=6, $j_{max}$=6).*

The velocities in the *x*-coordinate direction, $u_{i,j}$, in the cells of the calculation domain, are calculated on the right hand edges of the cells, the velocities in the *y*-direction, $v_{i,j}$, are calculated on the upper edges of the cells, and the pressure, $\overline{p}_{d_{i,j}}$, is calculated in the middle of the cells, in order to avoid pressure fluctuations during the iteration process.

A calculation domain surrounded by one row of ghost cells is depicted in Figure 4. The ghost cells are used to define boundary conditions at the edges of the calculation domain. Equations (24) and (25) can now be discretized with respect to position:

$$u_{m_{i,j}}^{(n+1)} = F_{i,j}^{(n)} - \frac{\Delta t}{\rho}\frac{\left(\overline{p}_{d_{i+1,j}}^{(n+1)} - \overline{p}_{d_{i,j}}^{(n+1)}\right)}{\Delta x}, i = 2,...,i_{\max}+1,\ j = 2,...,\ j_{\max}+1 \tag{26}$$

$$v_{m_{i,j}}^{(n+1)} = G_{i,j}^{(n)} - \frac{\Delta t}{\rho}\frac{\left(\overline{p}_{d_{i+1,j}}^{(n+1)} - \overline{p}_{d_{i,j}}^{(n+1)}\right)}{\Delta y}, i = 2,...,i_{\max}+1,\ j = 2,...,\ j_{\max}+1 \tag{27}$$

where *F* and *G* are discretized at the right and upper walls of the cells respectively.

**Solution of the Poisson-type equation**

In order to solve pressure at the new time step, the continuity equation (12) is first written as follows:

$$h\frac{\partial u_m}{\partial x} + u_m\frac{\partial h}{\partial x} + h\frac{\partial v_m}{\partial y} + v_m\frac{\partial h}{\partial y} + \frac{\partial h}{\partial t} = 0\,. \tag{28}$$

The velocity field $\left(u_m^{(n+1)}, v_m^{(n+1)}\right)^T$ from Equations (26) and (27) is now inserted into Equation (28) and the following Poisson-type equation can be written:

$$h\frac{\partial^2 \overline{p}_d^{(n+1)}}{\partial x^2} + h\frac{\partial^2 \overline{p}_d^{(n+1)}}{\partial y^2} + \frac{\partial h}{\partial x}\frac{\partial \overline{p}_d^{(n+1)}}{\partial x} + \frac{\partial h}{\partial y}\frac{\partial \overline{p}_d^{(n+1)}}{\partial y} =$$

$$\frac{\rho}{\Delta t}\left(h\frac{\partial F^{(n)}}{\partial x} + h\frac{\partial G^{(n)}}{\partial y} + \frac{\partial h}{\partial x}F^{(n)} + \frac{\partial h}{\partial y}G^{(n)} + \frac{\partial h}{\partial t}\right). \tag{29}$$

The Poisson-type equation can now be discretized, which results in the following set of linear equations, which have $i_{max} \cdot j_{max}$ unknown values of $\overline{p}_{d_{i,j}}$, $i=1,\ldots,i_{max}$, $j=2,\ldots,j_{max}$, which have to be solved by using a suitable algorithm, like the Gauss-Seidel method:

$$A_{W_{i,j}}\overline{p}_{d_{i-1,j}}^{(n+1)} + A_{P_{i,j}}\overline{p}_{d_{i,j}}^{(n+1)} + A_{E_{i,j}}\overline{p}_{d_{i+1,j}}^{(n+1)} + A_{N_{i,j}}\overline{p}_{d_{i,j+1}}^{(n+1)} + A_{S_{i,j}}\overline{p}_{d_{i,j-1}}^{(n+1)} = B_{i,j}\,, \tag{30}$$

where

$$A_{W_{i,j}} = \frac{h^n_{c_{i,j}}}{\Delta x^2} - \frac{h^n_{u_{i,j}} - h^n_{u_{i-1,j}}}{2\Delta x^2},\ A_{P_{i,j}} = -\frac{2h^n_{c_{i,j}}}{\Delta x^2} - \frac{2h^n_{c_{i,j}}}{\Delta y^2},\ A_{E_{i,j}} = \frac{h^n_{c_{i,j}}}{\Delta x^2} + \frac{h^n_{u_{i,j}} - h^n_{u_{i-1,j}}}{2\Delta x^2}$$

$$A_{N_{i,j}} = \frac{h^n_{c_{i,j}}}{\Delta y^2} + \frac{h^n_{v_{i,j}} - h^n_{v_{i,j-1}}}{2\Delta y^2},\ A_{S_{i,j}} = \frac{h^n_{c_{i,j}}}{\Delta y^2} - \frac{h^n_{v_{i,j}} - h^n_{v_{i,j-1}}}{2\Delta y^2} \text{ and}$$

$$B_{i,j} = \frac{\rho}{\Delta t}\left( h^n_{c_{i,j}} \frac{F^n_{i,j} - F^n_{i-1,j}}{\Delta x} + h^n_{c_{i,j}} \frac{G^n_{i,j} - G^n_{i,j-1}}{\Delta y} \right) +$$

$$\frac{\rho}{\Delta t}\left( \frac{h^n_{u_{i,j}} - h^n_{u_{i-1,j}}}{\Delta x} \frac{F^n_{i,j} - F^n_{i-1,j}}{2} + \frac{h^n_{v_{i,j}} - h^n_{v_{i-1,j}}}{\Delta y} \frac{G^n_{i,j} - G^n_{i,j-1}}{2} + \frac{h^{(n+1)}_{c_{i,j}} - h^n_{c_{i,j}}}{\Delta t} \right),$$

where the subscripts in $h_c, h_u$ and $h_v$ indicate that the height of the gap is calculated at the center of the cell, at the right edge of the cell, and at the upper edge of the cell, respectively.

After the pressure in the cells of the calculation domain has been calculated at the new time step $t_{n+1}$, the new values for the velocity components $u^{(n+1)}_{m_{i,j}}$ and $v^{(n+1)}_{m_{i,j}}$ can be calculated by using the discretized equations of motion (26) and (27). The iteration continues now until a preset value for the *L2*-norm of the change of velocity between iteration cycles has been achieved. The *L2*-norm is defined as

$$\left\| r^{it} \right\|_2 := \left( \frac{1}{i_{\max} j_{\max}} \sum_{i=1}^{i_{\max}} \sum_{j=1}^{j_{\max}} \left( r^{it}_{i,j} \right)^2 \right)^{1/2} \tag{31}$$

where $r^{it}_{i,j}$ is the change of the velocity in the *x*-coordinate direction, $u^n_{i,j} - u^{n-1}_{i,j}$, between the successive iteration cycles.

**The boundary conditions**

The symmetric and periodic boundary conditions were used in this study.

Symmetric boundary

The symmetry boundary condition can be assigned e.g. for the lower edge of the calculation domain shown in Figure 4 by setting:

$$
\begin{aligned}
u_{m_{i,1}} &= u_{m_{i,2}} \\
v_{m_{i,1}} &= 0 \\
\overline{p}_{d_{i,1}} &= \overline{p}_{d_{i,2}}
\end{aligned}
\tag{32}
$$

Periodic boundary

The periodic boundary condition can be assigned e.g. for the left edge of the calculation domain shown in Figure 4 by setting:

$$
\begin{aligned}
u_{m_{1,j}} &= u_{m_{i\max+1,j}} \\
v_{m_{1,j}} &= v_{m_{i\max+1,j}} \\
\overline{p}_{d_{1,j}} &= \overline{p}_{d_{i\max+1,j}}
\end{aligned}
\tag{33}
$$

## CALCULATIONS

A rectangular ice floe with dimensions 1 m x 1 m and a ball-shaped hull form with $R_x$ = 75 m and $R_y$ = 75 m was the chosen geometry for the analysis. The ice floe is assumed to be located symmetrically on the moving hull surface. The ball-shaped hull form was approximated by the following equation:

$$
h \approx h_0 + \frac{x^2}{2R_x} + \frac{y^2}{2R_y}, \tag{34}
$$

where $h_0$ is the distance of the hull and the ice floe at the origin. The origin was placed in the middle of the ice floe. Due to symmetry, half of the ice floe ( $y \geq 0$ ) was chosen to be the calculation domain. The minimum distance between the hull surface and the ice floe, $h_0$, was given a value of 0.0001 m. The symmetric boundary condition was set at the edge $y$ = 0. It was assumed that the neighbouring ice floes are of the same size as the floe in question, and thus periodic boundary conditions given in equations (33) were set at the inlet ($x$ = -0.5 m) and at the outlet ($x$ = 0.5 m). At the edge $y$ = 0.5 m a symmetric boundary condition was set. The velocity of the hull was 5 m/s in the $x$-coordinate direction. The fluid in the gap was water at 0°C, $\rho = 1000$ kg/m$^3$ and $\eta$ = 0.001792 Pa·s . The flow in the gap is thus predominantly turbulent, the maximum local Couette Reynolds number being about 4700, and the minimum about 140. The turbulence model of Hirs was used in the calculations. An equidistant grid with $i_{max}$ x $j_{max}$ = 50 x 25 was used, giving a grid spacing of 0.02 m.

| Mass flow at the inlet [kg/s] | Average pressure in the gap, $\tilde{p}_d^*$ [Pa] | Moment about the $y$-axis [Nm] |
|---|---|---|
| 1.110243 | -2045.4 | 1323.4 |

**Table 1.** The results of the calculations.

The results of the calculations are shown in Table 1. The pressure distribution in the gap is depicted in Figure 5. The pressure field is characterized by high positive and negative pressure peaks. Because of inertia effects, the absolute value of the negative pressure peak is higher than the positive pressure peak, which can be seen in Figure 6. For this reason, the average pressure, $\tilde{p}_d^*$, in the gap is negative. Since the pressure distribution in the gap is asymmetric with respect to the *y*-axis, a positive (clockwise) moment is generated on the ice floe (see Table 1). This means that the ice floe has to be supported by the shear forces, *Q*, between the ice floe and the adjacent ice floes in order to maintain its position.

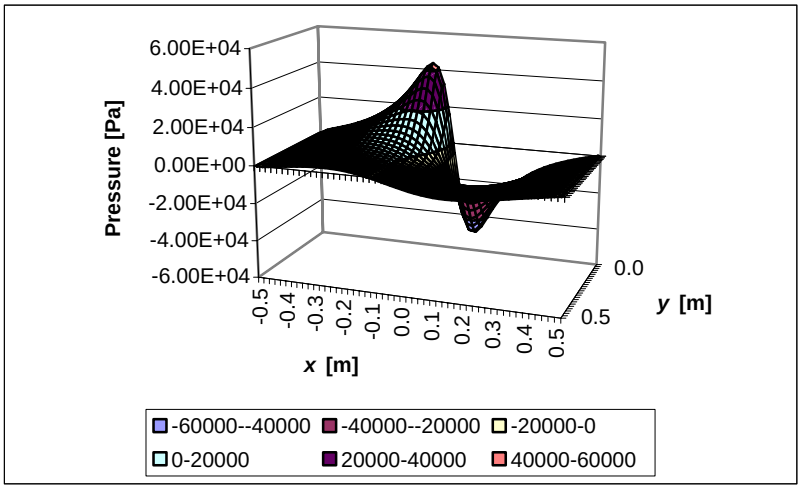


**Figure 5.** The pressure distribution in the gap. The inlet is on the left-hand side, the outlet on the right-hand side, the centreline at the back of the figure, and the outer edge of the ice floe is in the foreground of the figure.

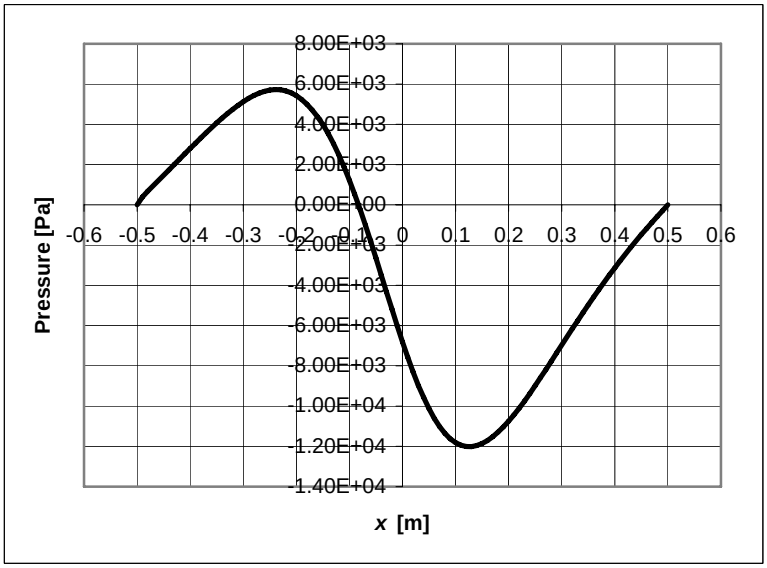


**Figure 6.** The distribution of the pressure, $\overline{p}_d$, at section y = 0.24 m.

## Variation of the speed of the hull surface

The speed of the hull surface was varied from 1 m/s to 6 m/s. The other parameters were the same as given above. The effect of the speed of the hull surface on the average pressure in the gap is shown in Figure 7.

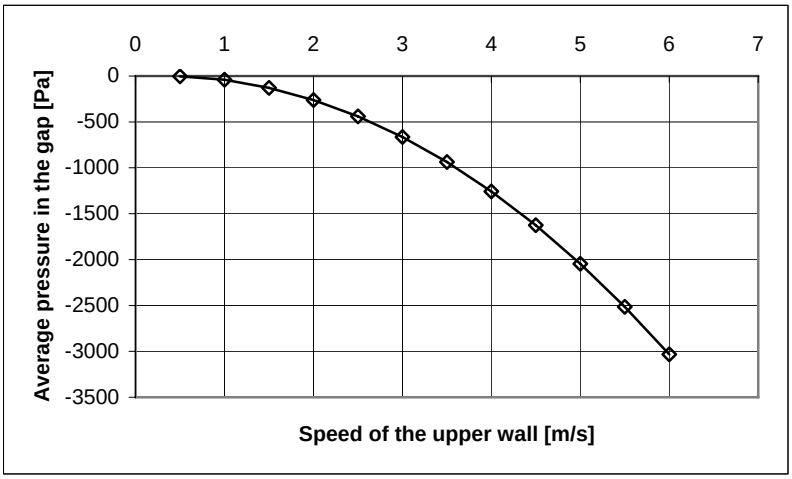


**Figure 7.** The effect of the speed of the hull surface on the average pressure in the gap.

## The effect of the inclination of the ice floe on the pressure in the gap

The case where the gap is not symmetrical but inclined with respect to the *y*-coordinate axis is now considered. This is achieved by shifting the contact point of the ice floe with the hull surface forwards or backwards along the *x*-coordinate axis. The gap is thus still symmetrical with respect to the *x*-coordinate axis. Two cases where the flow is assumed to be periodic, as depicted in Figure 8, are now considered. In Case 2 the gap at the inlet is larger than the gap at the outlet. In Case 3 the gap at the inlet is smaller than the gap at the outlet. The other parameters were the same as in the previous calculations. The results of the analysis are shown in Figure 9.

In Figure 9 the significant effect of the position of the ice floe on the average pressure in the gap can be observed. If the inclination angle is -0.23 degrees (the contact point of the ice floe is moved 0.15 m in the negative *x*-coordinate direction), a considerable decrease in pressure can be seen to exist in the gap, whereas if the inclination angle is 0.23 degrees (the contact point of the ice floe is moved 0.15 m in the positive *x*-coordinate direction), a considerable increase in pressure exists in the gap.

The turning moment on the ice floe resulting from the pressure in the gap is always positive. This means that the pressure distribution in the gap seems to favour Case 2. In ice model tests in thick ice the layer of broken ice floes is quite stable and the floes keep together. However, at high speed in thin level ice the broken ice floes do not stay together under the hull but stray further away from the hull quite early, and result in “a cloud” of ice floes around the hull of the ship. This phenomenon may be at least partly

explained by the positive moment due to asymmetric pressure distribution in the gap between the hull and the ice floes.

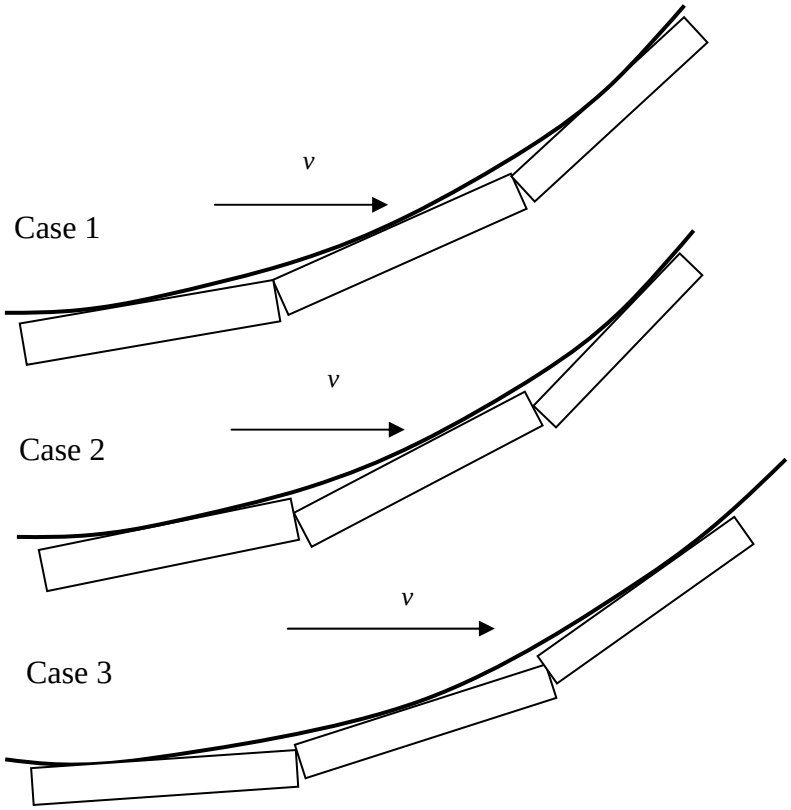


**Figure 8.** The considered cases with an inclined ice floe.

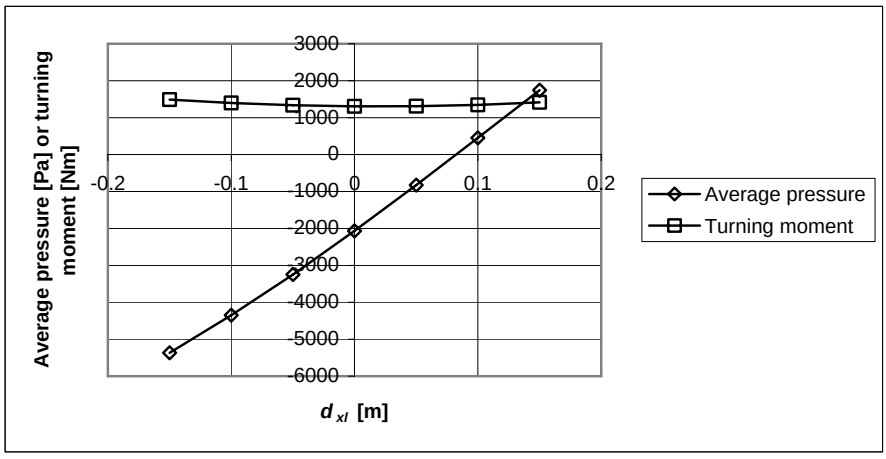


**Figure 9.** Average pressure in the gap, $\tilde{p}_d^*$, and the turning moment about the y-coordinate axis for the inclined ice floe resulting from the pressure in the gap. The distance of the contact point of the ice floe and the hull surface measured from the centre of the ice floe is $d_{xl}$.

## CONCLUSIONS

The flow in the gap between the hull surface and ice floes may cause considerable changes in pressure in the gap. The existence of this phenomenon requires a continuous shear-driven flow of water in the gap between the hull surface and the ice floes. Under favourable conditions this may cause a considerable decrease in pressure in the gap, see Kämäräinen (1993) and (2007). However, the existence of low average pressure in the gap is very sensitive to the position of the ice floes with respect to the hull surface.

## ACKNOWLEDGEMENTS

Emeritus Professor Eero-Matti Salonen has been my advisor in my studies on the pressure decrease phenomenon since 1993. I warmly thank him for his continuous and patient advice, encouragement, and support during the course of my studies.

## REFERENCES

Constantinescu V.N., and Galetuse S. (1974). On the Possibilities of Improving the Accuracy of the Evaluation of Inertia Forces in Laminar and Turbulent Films. *Journal of Lubrication Technology*, July 1974, pp. 69 - 79.

Constantinescu V.N. and Galetuse S. (1982). Operating Characteristics of Journal Bearings in Turbulent Inertial Flow. *Journal of Lubrication Technology*, April 1982, Vol. 104, 173 - 179.

Griebel M., Dornseifer Th., and Neunheffer T. (1998). *Numerical Simulation in Fluid Dynamics.* A Practical Introduction. The Society for Industrial and Applied Mathematics, 1998.

Hirs G.G. (1973). Bulk Flow Theory for Turbulence in Lubricant Films, *Trans. ASME,* series F, vol. 95, 137 – 146.

Kämäräinen J. (1993). *On the Speed Dependence of the Ice Submerging Resistance in Level Ice*. Helsinki University of Technology, Faculty of Information Technology, Computational Dynamics, Otaniemi 1993/38.

Kämäräinen J. (2007). *Theoretical Investigation on the Effect of Fluid Flow between the Hull of a Ship and Ice Floes on Ice Resistance in Level Ice.* Doctoral Dissertation, TKK Dissertations 80, Helsinki University of Technology, 2007.

Leschziner M.A. (1976). *Turbulent flow in finite width bearing films including turbulent transport and inertia effects*. Thesis submitted for degree of Doctor of Philosophy in the Faculty of Engineering, University of London, August 1976.

Puntigliano F.M. (1995).*On the resistance components below the waterline in the continuous mode of icebreaking - model tests.* HSVA Report No. E253/95.

Puntigliano F.M. (2000). Ice Performance of the MPV Neuwerk. *On the Low Pressure Phenomenon between Ice and Hull, Full-Scale Trials, Physical and Mathematical Modelling.* HSVA Report No. 1640 Part B.

Schlichting H., and Gersten K. (2000). *Boundary-Layer Theory,* 8th Revised and Enlarged Edition, Springer, 2000.

Valanto P. (1989). *Experimental and Theoretical Investigation of the Icebreaking Cycle in Two Dimensions.* Thesis for the degree of Doctor of Philosophy, University of California at Berkeley.

Jorma Kämäräinen, merenkulunylitarkastaja

Merenkulkulaitos
PL 171, 00181 Helsinki
email: jorma.kamarainen@fma.fi